Concentration Fluctuations in a Stirred Baffled Vessel

F. S. MANNING and R. H. WILHELM

Princeton University, Princeton, New Jersey

A stirred vessel is maintained in a quasisteady state by continuously introducing water and a conductive tracer solution and continuously removing the resulting mixture by overflow. Detailed properties of the system are elucidated by measuring tracer concentration changes with a conductivity probe in a volume element of the order of 0.3 cu. mm. By the use of suitable electronic equipment the following statistical concentration parameters are measured in experiments with three diameters of flat-bladed turbines and with a tenfold range of rotational speed: temporal mean, total root-mean-square fluctuation, spectral distribution of fluctuations, and Eulerian micro time scale. Results are interpreted in terms of behavior of time-average and fluctuation measures in three regions, the generation region within the impeller volume, the decay region which starts in the horizontal fluid sheet issuing from the impeller, and the recirculation flow region in the vessel.

Generation of concentration fluctuations within the confines of the impeller is described in terms of a model involving gross mixing, without significant decay, in the wake of each flat blade. Distributions of mean and fluctuating concentrations are suggested to provide a measure of uniformity in the vessel as a whole. The former, in particular, was remarkably constant throughout the vessel.

Fluid mixing is of central importance in the transport, reaction, and separation processes of chemical technology. Intermingling of fluids in a turbulent field involves the simultaneous processes of transport and of mixing, the former being the transfer of matter under a concentration gradient and the latter the rate of progress of the system toward the equilibrium state of complete randomness at the molecular level. Although the art of mixing has advanced greatly, the science of mixing, as part of turbulence theory, is in an early state of development. There is need to elucidate experimental turbulence mixing characteristics in physical arrangements of technological interest as well as in fluid mechanically idealized systems.

Empirical approaches to the characterization of stirred vessels have dominated the field. Some studies have related to the gross effect of liquid mixing on certain processes occurring in the vessel and others to more local effects of mixing, such as the dispersal of a tracer. Experimental criteria that have been suggested for characterizing the mixing efficiency of stirred vessels are these: power adsorption per unit volume (*19*); rate of dissolution or reaction (*9, 11, 17*); suspension of insoluble particles (*10, 21*); emulsification of immiscible liquids (*4*); gas dispersion (*6*); adsorption of a dye (*8*); increase of interfacial area (*18*); damping of input fluctuations (*7*); and mixing time for tracers (*12, 15, 20, 22*).

Recent theoretical studies include that of Corrsin (*5*) on an idealized turbulent mixer, of Batchelor (*1*), Batchelor, Howells, and Townsend (*2*) and Beek and Miller (*3*) on scalar property fluctuations.

This work is an exploratory study of mixing of miscible liquid streams in a fully baffled, stirred vessel. A steady state condition is generally achieved by the introduction of a conductivity tracer sodium chloride solution into a stream of water which flows slowly upward through the stirred vessel. A conductivity probe (*16*) which sees concentration changes in a volume of the order of 0.3 cu. mm. is used. Spatial variations of the following concentration properties were measured: temporal mean value, root-mean-square fluctuation, and spectral distribution function. The probe permits characterization of mixing turbulence characteristics which are microscopic relative to the vessel size but are coarse compared with the fine-grained structure that is significant in chemical reaction. The probe thus permits definition of gross scale distributions in mixing devices; it also permits partial description of the large-scale end of the cascade process that is mixing. Present results do not conform to sufficiently

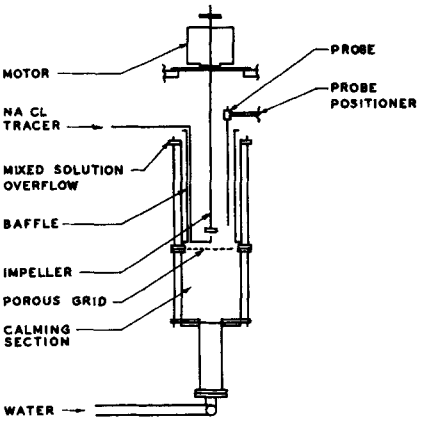

Fig. 1. Stirred vessel.

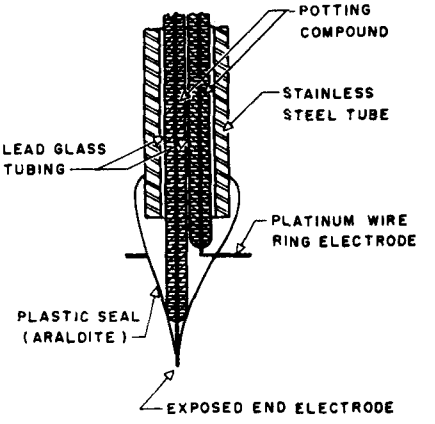

Fig. 2. Conductivity probe tip.

F. S. Manning is at Carnegie Institute of Technology, Pittsburgh, Pennsylvania.

idealized conditions to justify comparison with current theories.

THEORY

This section is restricted to defining terms involved in data reduction.

Intensity

Turbulent intensity is defined as

$$[(1/3)(\overline{u_i^2} + \overline{u_j^2} + \overline{u_k^2})]^{1/2}/Q = u_o/Q \quad (1)$$

Microscale

The Eulerian micro time scale, which is a measure of the most rapid changes

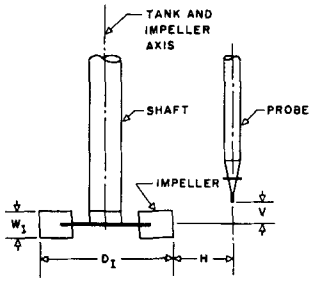

D_I DIAMETER OF IMPELLER, INCHES.
W_I WIDTH OF IMPELLER BLADE, INCHES
H HORIZONAL SEPARATION DISTANCE FROM TIP OF IMPELLER TO POINT ELECTRODE OF PROBE, INCHES.
V VERTICAL DISTANCE FROM CENTER OF IMPELLER BLADE TO TIP OF PROBE, INCHES.
H/D DIMENSIONLESS SEPARATION DISTANCE.
V/W_I DIMENSIONLESS VERTICAL DISTANCE.

Fig. 3. Elevation view of impeller and probe positions.

that occur in the fluctuating velocity component u_i, is defined by

$$\frac{1}{\lambda_T^2} = \frac{1}{2u_o^2}\overline{\left[\frac{\partial u_i}{\partial t}\right]^2_{t=0}} \quad (2)$$

Liepmann and Robinson (*14*) related the Eulerian micro time scale to the zero count. The following assumptions were made:

1. There is no correlation between the fluctuating velocity and its time derivative.
2. The probability distributions of the fluctuating velocity and its time derivative are normal.

Then

$$N_o = (2)^{1/2}/(\pi\lambda_T) \quad (3)$$

Spectrum

The concentration spectral distribution function $G(k)$ is defined as

$$\overline{(\Delta C^2)} = \int_o^\infty G(k)dk \quad (4)$$

or

$$G(k)/\overline{(\Delta C^2)} = \overline{(\Delta C_k^2)} \quad (5)$$

Another distribution function now is defined:

$$\Phi^2 = \overline{(\Delta C_f^2)}/\overline{(\Delta C^2)} \quad (6)$$

The wave number and the frequency are related:

$$k = 2\pi n_f Q \quad (7)$$

Hence

$$G(k)/\overline{(\Delta C^2)} = (Q/2\pi)\Phi^2 \quad (8)$$

Present results are reported in terms of Φ. Selectivity of the wave analyzer is a known fraction of the frequency to which it is tuned rather than a unit step. The spectral distribution function therefore is obtained by correcting the wave analyzer output (ΔC_{fo}) for the actual band pass width as follows:

$$\Delta C_f = (\text{B.P.F.})\ (\Delta C_{fo}) \quad (9)$$

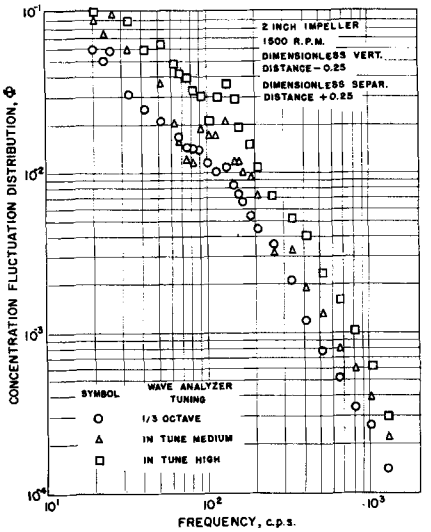

Fig. 4. Calculated Φ for three selectivities.

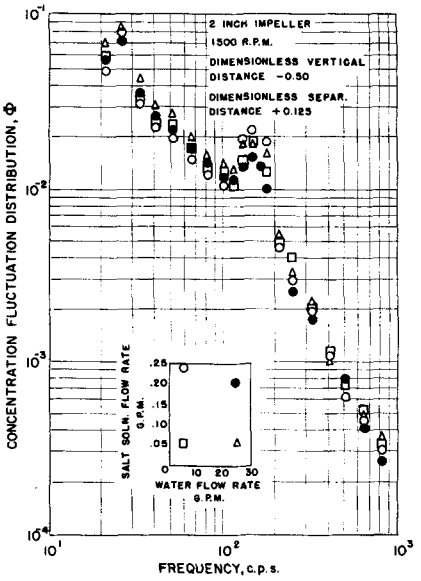

Fig. 5. Effect of flow rates on concentration fluctuations.

EXPERIMENTAL

A description of equipment, experimental procedure, reduction of data, and equipment characteristics is presented here in brief; details are given elsewhere (*13, 16*).

Equipment

A mixing vessel and a conductivity probe with attendant electronic circuitry are described.

The mixing vessel is shown in Figure 1. Tap water is pumped through a rotameter into a calming section, through the cylindrical primary mixing column which

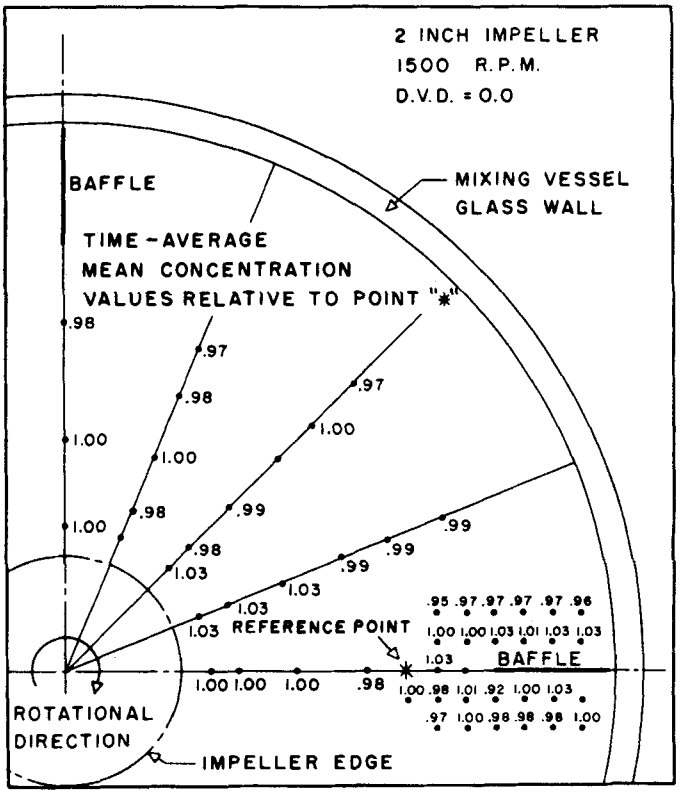

Fig. 6. Uniformity of mean concentration with horizontal angular position.

is 9.5 in. I.D. by 17 in. long, and finally into the overflow section. The mixing section is separated from the calming section by a grid containing many closely spaced holes. A 0.9 N sodium chloride tracer is introduced continuously just below the centrally located, six-bladed turbine impeller, that is into the cylindrical hole (Figure 7) formed by the rotating blades. A variable speed motor drives the impeller. rotational speed is measured by means of a strobotac. The vessel is provided with four, symmetrically placed, 1-in. wide baffles.

The conductivity probe (tip shown in Figure 2) consists of a small and large electrode formed from 26-gauge platinum wire; the small electrode is the exposed end cross section of one wire, and the other electrode is a circular wire loop. The size ratio is 200:1. The electrode assembly is encased in a grounded, stainless steel tube to minimize extraneous effects on primary probe readings of other grounds that are present in the mixing vessel. The interior volume of the probe assembly was filled with potting compound to prevent internal vibration of the platinum wires.

The probe was placed in position within the stirred vessel by means of a compound vise assembly and was calibrated by immersion in a series of static, standard sodium chloride solutions in the vessel; the calibration did not change as the result of stirring. Voltage output of the probe is linear in concentration. However the presence of objects at ground potential proved to have significant effects; these contributions were compensated for by calibration of the probe while it was positioned in the stirred vessel.

Circuitry consisted of these units: probe, signal oscillator (set to 15 kc.), a.c. amplifier, rectifier, wave analyzer, d.c. amplifier, squaring circuit, averaging circuits, strip-chart recorder, and suitable voltmeters. This assembly is used to measure temporal mean concentrations of about 0.005 N sodium chloride within 1% accuracy; total root mean square concentration fluctuations between 0.3 and 30% of the mean concentration and within 0.05% of the mean value; spectral energy distribution functions between 5 and 1,500 cycles/sec.; and Eulerian micro time scales between 2 and 10 msec., within 5%.

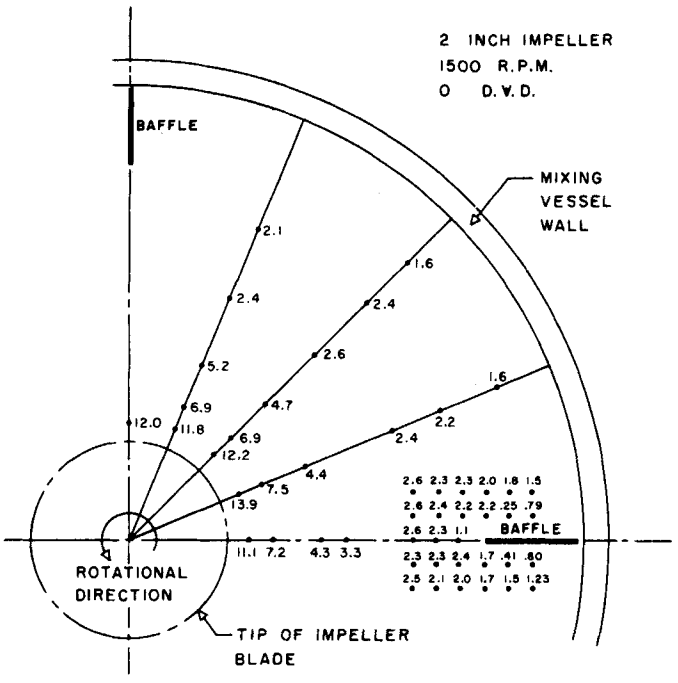

Fig. 8. Uniformity of root mean square concentration fluctuations with horizontal angular position including baffle effect.

Data Processing

Procedures for processing data are outlined here; distance is an independent dimensionless variable while dependent variables are average velocity, average concentration, root mean square concentration fluctuation, spectral distribution and Eulerian micro time scale.

Dimensionless position horizontal and vertical coordinates of the probe in the vessel are defined in Figure 3.

Average concentration and root mean square concentration fluctuations are both converted from corresponding voltage signals taking into account the cell constant and capacitance, sodium chloride solution temperature, and conductivity-concentration relation. The presence of grounds also is allowed for quantitatively. In addition the reduction of signal to root mean square concentration fluctuation involves calibration of squaring and integrating circuits by the procedure of substitution of voltage signals of known frequency and amplitude into the measuring circuit in place of the probe.

In converting the wave analyzer signal output to a spectral concentration distribution function it is necessary to reduce the analyzer output for any given distributed filter selectivity to an ideal unit wave number or unit frequency selectivity. This is shown in Figure 4. Although the average size of the signal does depend somewhat on the setting of the wave analyzer window, the significant features of the spectrum shape are retained at each setting. For convenience most measurements–including all reported in this paper–were made at the 1/3 octave setting.

Microscales are computed from Equation (3), and the counted number of traverses in a unit time of the signal voltage. The time elapsed for a count is taken at 1 sec., a time interval which assures that counts in succeeding intervals do not vary by more than 5%.

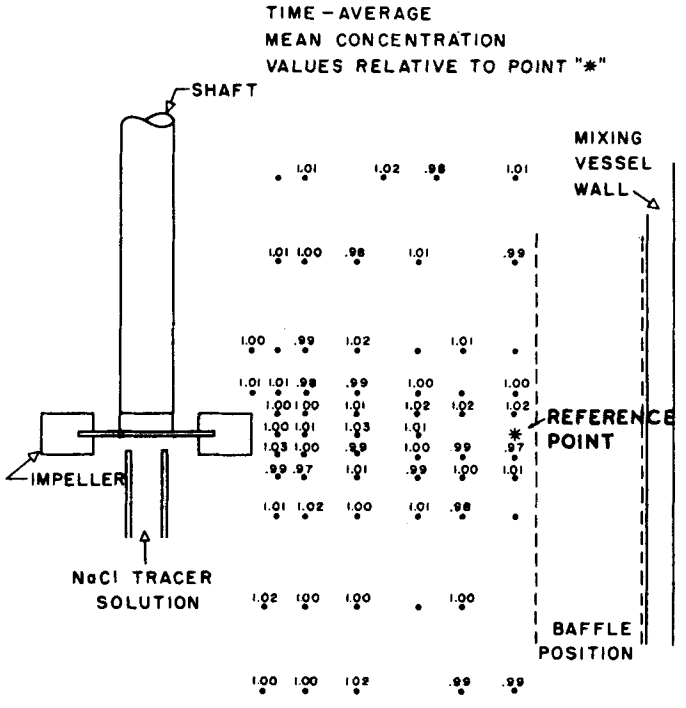

Fig. 7. Uniformity of mean concentration with geometrical position.

TABLE 1. RANGES OF EXPERIMENTAL VARIABLES

Measured variable	Temporal mean	Concentration, r.m.s.	Spectral variables	Microscale
Impeller size, in.	1, 2, 4	1, 2, 4	1, 2, 4	1, 2, 4
R.P.M.	286 to 2,860	286 to 2,860	286 to 1,500	286 to 2,860
D.S.D.	0.06 to 3.0	0.06 to 3.0	0.125 to 3.0	0.06 to 2.5
D.V.D.	−7.5 to +7.5	−14.0 to +5.0	−0.25	−14 to +5.0

Equipment Characteristics

Probe properties relate to capacitance, geometry, and discrimination. It is shown that total impedance of the probe is very nearly independent of carrier frequency to well beyond 15 kc. which was therefore chosen as the operation frequency. Such independence indicates that the capacitance contribution to the total impedance is negligibly small. The presence of a finite measuring device certainly disturbs local flows, but comparative experiments with probe tips of different shapes and lengths showed that such disturbances do not affect concentration measure significantly in the present work. Probe discrimination is the volume surrounding the probe within which the presence of a concentration nonuniformity (assumed spherical) will become evident as a measurable signal. The net effect of the presence of such nonuniformities at various positions in the electrical field is determined by measurement of impedance between the electrodes referred to the impedance when the disturbance is removed from the system. Such measurements were embodied in model tests from which it was determined that the region of discrimination sensitivity is approximately 5 probe volumes (*16*).

Mixing vessel characteristics are controlled by the impeller and by the continuous flow of water through the unit. Whether or not the assembly more closely resembles an agitated vessel or a pipe was determined by means of a set of four experiments in which concentration fluctuation spectral measurements were taken at the same point near the impeller for four combinations of high and low flow rates of water and sodium chloride tracer. Within experimental error substantially identical spectral distribution functions were obtained in the four experiments (see Figure 5). Similar behavior is expected farther from the impeller. It is concluded that stirrer rather than pipe flow characteristics prevail.

The noise was subtracted from the mean square value of the total signal by means of the following relationship:

$$\overline{(\text{net fluctuation})^2} = \overline{(\text{total fluctuation})^2} - \overline{(\text{noise fluctuation})^2} \qquad (10)$$

Noise is here defined as the probe voltage fluctuation for stirring conditions which are identical to those in primary operation but lack the addition of sodium chloride tracer solution. In all cases reproducible values of total signal and noise were obtainable. In addition noise levels were sufficiently low to permit quantitative measurement of the net fluctuation reproducible. It was found that the magnitude and character of the noise is unaffected by platinization of probe and conductivity of solution. Separate tests indicated that a major source of noise was mechanical vibrations, certain resonance frequencies (due to probe geometry) being evident. In usual operation the probe is buffeted by packets of fluid coming from the impeller.

RESULTS

Performance is discussed according to type of measurement. Since the stirred vessel has four symmetrically located baffles of equal size and a centrally positioned impeller, geometrical symmetry is realized for each quadrant in any horizontal plane. Measurement therefore is confined to one quadrant of the stirred vessel.

These parameters were constant: water flow rate (6.5 gal./min.), tracer flow rate, and concentration (0.05 gal./min. at 0.9 N. sodium chloride). Flat-bladed turbines with six blades, geometrically proportioned between sizes, were used. Ranges of experimental variables are summarized in Table 1.

The remarkable uniformity of the mean tracer concentration in horizontal and vertical traverses is evident in Figures 6 and 7, respectively.

Root mean square values of the total concentration fluctuation are shown (Figures 8 and 9) to be independent of angular position about the vessel axis and to vary only very locally near baffles. The variation of this concentration intensity in the horizontal plane at D.V.D. = 0 is shown in Figure 9. Similar intensity measurements at other horizontal plane positions above and below the impeller are represented typically by Figure 10. Difference in intensity above and below the impeller arises from the lack of symmetry between these regions. As is well known the horizontal fluid sheet issuing from the impeller divides into two vertical streams near the vessel wall. These two streams flow to form doughnut-shaped circulation patterns above and below the impeller, respectively. The nonsymmetry of concentration fluctuation intensities in these circulations arises because the lower stream is supplied with fresh water from the porous surface at the vessel bottom. This dilution causes much larger root mean square concentration fluctuations in the lower than upper sections, but the fluctuations in both are less than in the main fluid sheet.

The effect of impeller diameter on intensity at constant power dissipation per unit volume is presented in Figure 11. Highest intensity is associated with the smallest impeller. Variation of intensity with rotational speed at constant impeller diameter is illustrated in Figure 12. In this case highest intensity is associated with lowest rotational speed.

Spectral distribution functions for the 2-in. turbine impeller at three rotational speeds are given in Figure 13. Close to the impeller (D.S.D. of 0.125) a primary generation frequency is noted. In all cases the generation frequencies are six times the rotational speed because of the presence of six impeller blades. Figure 14 presents distribution functions for two impeller sizes operating at approximately the same rotational speed. All spectral functions determined in this work (of which the above is a sample which

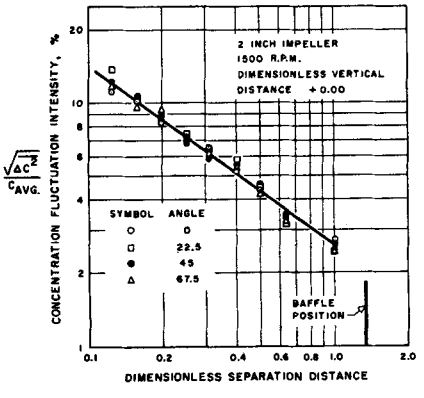

Fig. 9. Uniformity of root mean square concentration fluctuations with horizontal angular position.

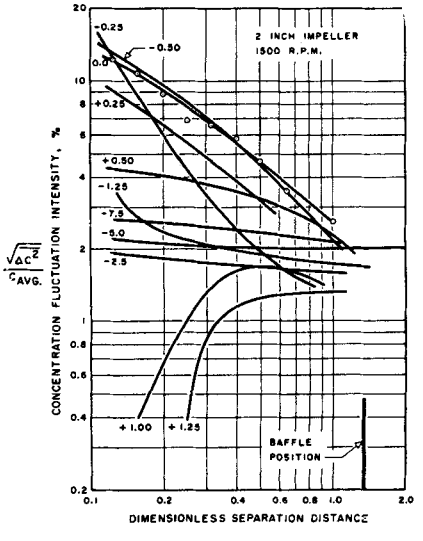

Fig. 10. Root mean square concentration fluctuation intensities for 2-in. impeller and 1,500 rev./min.

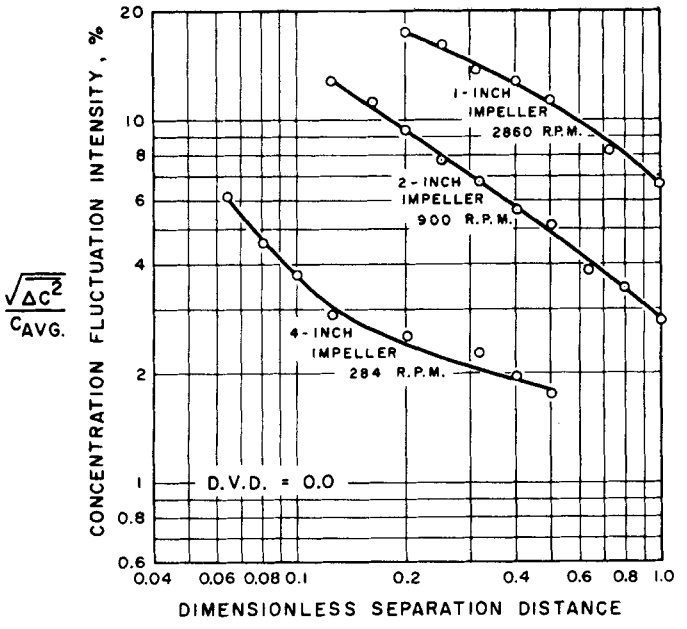

Fig. 11. Root mean square concentration intensities for varying impeller sizes and rotational speeds as constant power input.

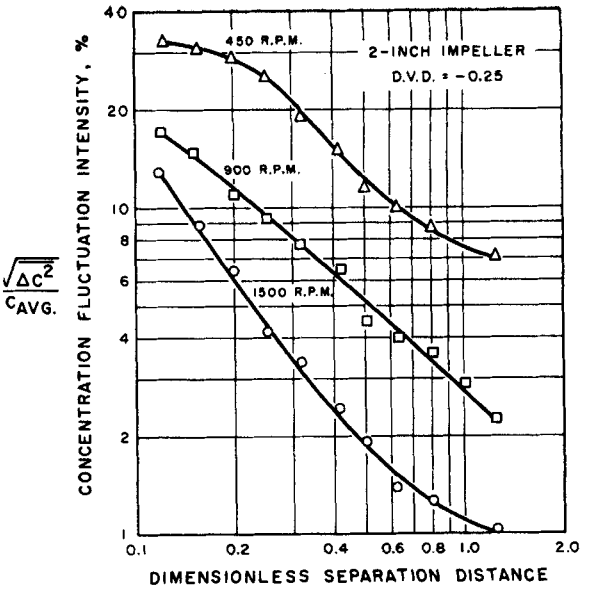

Fig. 12. Variation of root mean square concentration intensity with revolutions per minute for 2-in. impeller.

covered changes in impeller diameter, rotational speed, and probe position) were superimposable. That is no measurable progress is noted toward spectral decay.

Microscales are presented in Figures 15 and 16. The independence of angular position about the vessel in a horizontal plane through the center of the impeller blades is demonstrated in Figure 15. Similar behavior is noted at other horizontal plane levels. Again, baffle effects are shown to be local. The rising microscale-position curves represent data taken within or close to the fluid sheet issuing from the impeller and the level curves, well above and below the sheet. Change in microscale takes place only in the local region of the impeller. The microscales represented in Figure 16 correspond to length scales of approximately 1 cm. These are computed with mean velocities as measured by pitot tubes. These surprisingly high values, which result from lack of probe resolution and from insensitivity of recorder pen to frequencies above 200 cycles/sec., question the reliability of microscale measurement.

DISCUSSION

An interpretation of results starts with the premise that the impeller in its midsection produces a horizontal fluid sheet that retains its identity for some distance from the impeller before a jet type of interchange occurs at upper and lower edges (*16*). A two-dimensional water tunnel thus is formed having a decaying turbulence field which was generated in the impeller region. The action of the blades is suggested in effect to be analogous to the more common screen turbulence generators in wind tunnels. Thus in present experiments when a tracer is introduced at the impeller there results an initial distribution of both velocity and concentration intensities. Thereafter at succeeding lateral positions in the horizontal fluid sheet both velocity and concentration fields decay simultaneously.

Certain flow stream interdependencies determine the mean and fluctuation concentration characteristics of the system. The three streams involved are the fluid sheet (the volume rate of which is equal to the pumping rate of the impeller), the tracer stream, and the slow inlet water stream that enters through the porous bottom of the vessel and overflows at the top. The ratio of tracer to inlet stream determines the temporal mean concentration averaged over the volume of the tank. For convenience in characterizing compositional uniformity a stirred tank may be divided into two zones. One of these is the region of high velocity in and near the horizontal fluid sheet. The second relates to the regions above and below the level of the impeller in which gross recirculation takes place and which may not always be symmetric in behavior.

Two tools for characterizing uniformity suggest themselves to be the mean concentration and the concentration fluctuation intensity. The latter is the tool of greater discrimination and resolution. When one considers the fluid sheet, the value of the time-average concentration in the zone is established by the ratio of tracer to pumping rates and is found in all cases to be uniform. However the local mean concentration is not necessarily the same as the time and volume average over the whole vessel. Close agreement between these two values depends on the presence of a large mixing rate in the recirculation zone as well as in the impeller zone. Also, in the event of a large inlet flow compared with the impeller pumping rate, the entering fresh water which serves

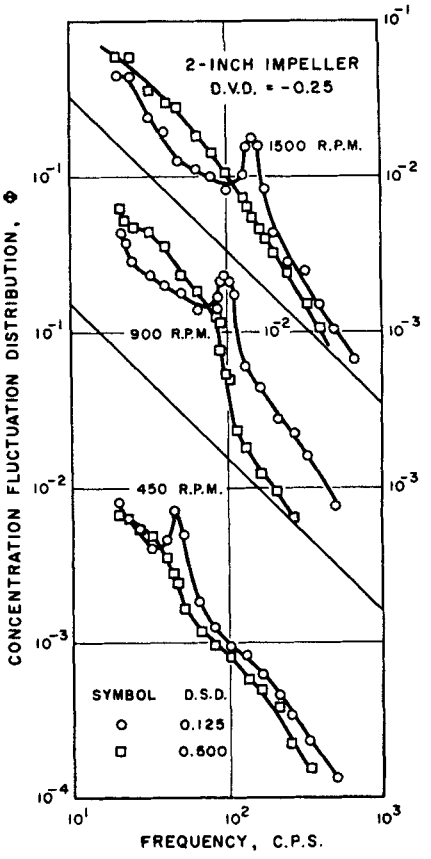

Fig. 13. Concentration fluctuation spectral distribution functions for 2-in. impeller at 1,500, 900, and 450 rev./min.

Table 2. Comparison of Experimental and Computed Ideal (Maximum) Concentration Fluctuation Intensities at Impeller Tip

Run no.	1	2	3	4	5	6	7
Impeller diameter, in.	1	1	2	2	2	4	4
Rev./min.	2,860	1,500	1,500	900	450	470	284
Tracer flow rate, v_t, gal./min.	0.05	0.05	0.05	0.05	0.05	0.05	0.05
Water flow rate, v_i, gal./min.	6.5	6.5	6.5	6.5	6.5	6.5	6.5
Recirculation rate, v_r, gal./min.	27	11.4	104	63	31	250	158
Concentration of NaCl in tracer stream C_t normality	0.855	0.855	0.855	0.855	0.855	0.855	0.855
Concentration of NaCl in recirculation stream C_r normality	0.0065	0.0065	0.0065	0.0065	0.0065	0.0065	0.0065
Mean concentration leaving impeller blade, C_e	0.00811	0.00955	0.00694	0.00721	0.00790	0.00670	0.00680
Ideal computed intensity, %	450	529	267	331	429	179	222
Experimental intensity, %	30.0	51.0	20.0	27.5	39.5	11.0	14.0

as a gross tracer produces local nonuniformities in the recirculation zones, especially in that below the impeller. The patterns of nonuniformity that may be uncovered by the inlet water tracer and detected by variation in time average concentration may be termed *distributions in the large*. Those nonuniformities that are detectable (as in the horizontal fluid sheet) by means of fluctuation intensities rather than by time-average concentrations are considered in the intermediate. Those local nonuniformities that are below the resolution level of the present probe and which are important in the ultimate mixing processes as the system progresses toward molecular uniformity are considered arbitrarily to be in the small.

The results of concentration fluctuation intensity measurements in the horizontal fluid sheet now are discussed in terms of the generation of the nonuniformities within the impeller boundaries.

Generation

Intensities at blade tip positions are determined within 5% by extrapolation of data. As a frame of reference an ideal intensity is identified as that which would be measured by a probe and attendant electronic gear of very high resolution. This intensity $(\overline{\Delta C^2_{id}})^{1/2}$, is based on the following model:

1. The recirculation stream entering the impeller from below is substantially at a time average composition C_r determined by the relative flow rates v_t, v_i and compositions C_t, C_i of the salt tracer stream and of the inlet water stream respectively:

$$C_r = \{C_t v_t + C_i v_i\}/(v_t + v_i) \quad (11)$$

2. The time-average composition C_e of the stream leaving the cylinder described by the impeller tips is determined by the relative flow rates v_t, v_r and compositions C_t, C_r of the salt tracer stream and of the recirculation stream respectively. The volumetric flow rate of the tracer stream is small compared with that of the recirculation pumping rate. Thus the change in the mean concentration on passing through the impeller is small but finite.

3. At steady state the small net increase in the time-average composition over the impeller is exactly balanced by a corresponding decrease as the fluid elements circulate outward to the wall and thence in a generally doughnut path, ultimately re-entering at some point in the intake region of the impeller. During this journey the recirculating stream becomes intermixed with the fresh water of the entering stream. It should be noted that in neither entering or exit streams of the impeller is there implication of constancy in local composition; each stream may well carry in the circulation loop a residue of previous disturbances that has not yet been attenuated.

4. The impeller blade region is considered to be a complex, local stirrer with contributions due to local recirculation between blades as behind any bluff object in a flow stream; sheeting out or strain deformation that occurs on the low pressure, upstream side of each blade; and spreading of the separation sheets that issue from the impeller tips.

5. It is assumed that in these local stirred vessels the entering recirculation and tracer streams become intermixed. The stream leaving consists of a taffylike composite of the two component streams. The mean concentration of the exit stream is

$$C_e = (C_r v_r + C_t v_t)/(v_r + v_t) \quad (12)$$

The ideal root mean square fluctuation about this mean concentration is

$$(\overline{\Delta C^2_{id}})^{1/2} = [\{v_r(C_r - C_e)^2 + v_t(C_t - C_e)^2\}/(v_r + v_t)]^{1/2} \quad (13)$$

Table 2 provides a comparison between computed ideal intensities and those obtained by extrapolation of intensity data to the blade edges. In this table all quantities were measured directly except recirculation rate and concentrations of tracer in recirculation stream entering and leaving the

Table 3. Characteristic Times of Mixing Vessel

Time	Average magnitude, sec.
Vessel holdup time	48
Impeller recirculation time	4
Contract time at impeller	1×10^{-3}
Decay time of generating frequencies	6×10^{-3}

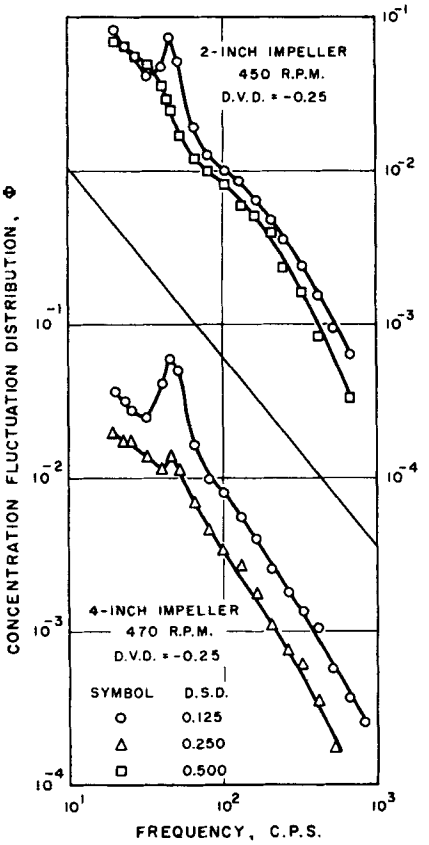

Fig. 14. Concentration fluctuation distribution functions for 2- and 4-in. impellers at 450 and 470 rev./min. respectively.

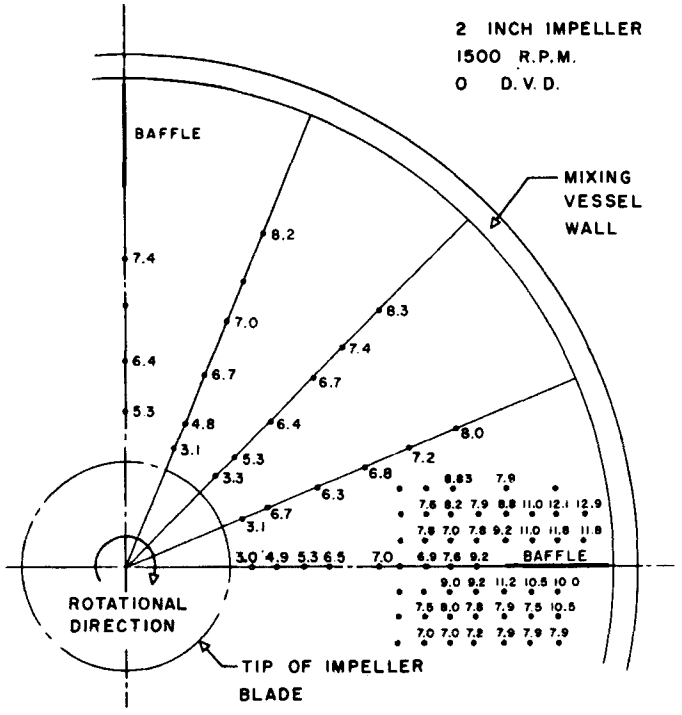

Fig. 15. Uniformity of concentration fluctuation Eulerian micro time scale with change in horizontal angular position.

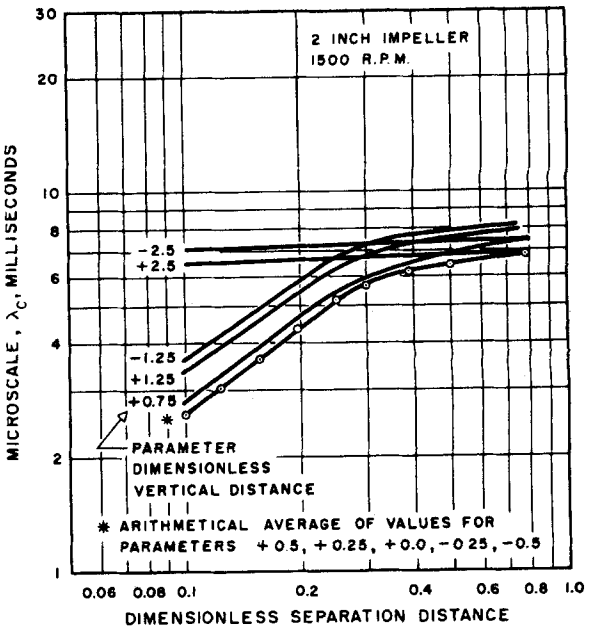

Fig. 16. Concentration fluctuation Eulerian micro time scale for 2-in. impeller and 1,500 rev./min.

impeller. Recirculation rate is estimated from the following relationship:

$$\text{Rate, } v_r = \pi^2 d_i^2 N_r d_w \qquad (14)$$

The compositions referred to were computed from Equations (11) and (12).

The linear relation on a log-log plot between ideal and experimental intensities provides a convenient design method that is valid over large ranges of compositions and flow rates. The two orders of magnitude difference between computed (ideal) and experimental intensities is suggested to be due to the large size of the probe with its consequent lack of resolution for measuring the number of strain-caused sheets of tracer material per unit volume and their strength. The formation of such sheets in the turbulent mixing of a scalar property as well as their subsequent dissipation by molecular diffusion has been suggested by Batchelor (*1*).

A marked similarity between the flow patterns of stirred vessels (flat-bladed turbine impeller) and water tunnels may be noted. Both have zones of turbulence decay, recirculation, and turbulence regeneration. Three characteristic holdup times are evident: the large average holdup time in the entire vessel (volume of vessel divided by net flow through rate, that is inlet water rate); the intermediate average recirculation holdup time (volume of vessel divided by impeller pumping rate); and the small contact time (volume space between impeller blades divided by impeller recirculation rate) in the continuously stirred flow pockets that constitute the impeller zone. Additional characteristic times are the initial decay time of the principal generation frequencies and the decay time of all fluctuations to the molecular scale. Table 3 gives orders of magnitude of some of these times.

SUMMARY

As a result of this exploratory study that involves application of a newly devised small volume conductivity probe to an industrially important device (a stirred, baffled vessel) these conclusions ensue:

1. The probe has sufficient resolution to determine the mean concentration, several measures of concentration fluctuation, and their spacial distribution.

2. Such measures suggest themselves to constitute a new criterion of effectiveness of turbulence generation and distribution in the engineering design of such devices. However indication can be given only of the initial stages of the turbulent mixing, and therefore the criterion is somewhat crude.

3. The present probe is insufficient in resolution to distinguish between current theories of turbulent mixing even if it were applied to a more ideal fluid mechanical system, for example a water tunnel or center of a pipe.

ACKNOWLEDGMENT

This work was supported by generous financial aid in the form of a research assistantship by The Shell Development Company and of fellowships by The Consolidation Coal Company and The Celanese Corporation of America.

NOTATION

B.P.F. = wave analyzer band pass factor [Equation (9)]
C = concentration of solute in solution
C_{avg} = time average mean concentration
C_e = concentration of stream leaving impeller
C_i = concentration of fresh tap water stream, that is, zero
C_r = concentration of recirculating stream
C_t = concentration of tracer stream
ΔC = concentration fluctuation
ΔC_f = fraction of the total concentration fluctuation per unit frequency (cycles/sec.) step, that occurs at the chosen frequency n_f
ΔC_{fo} = fraction of the total fluctuation that is not filtered out by wave analyzer when it is turned to the chosen frequency n_f
ΔC_{id} = theoretical maximum concentration fluctuation
ΔC_k = fraction of the total concentration fluctuation per unit wave number step that occurs at the chosen wave number k
D.S.D. = dimensionless separation distance, defined in Figure 3
D.V.D. = dimensionless vertical distance, defined in Figure 3
d_i = diameter of flat-bladed turbine impeller
d_w = blade width of flat-bladed turbine impeller

G = three dimensional spectral energy distribution function for the scalar fluctuations, Equation (4)
k = wave number, cm.$^{-1}$
N_r = rotational speed of impeller
N_o = zero count for turbulent fluctuations, that is the number of times a second that the turbulent fluctuation crosses zero
n_f = frequency, cycles/sec.
Q = absolute value of mass velocity
t = time
u_i, u_j, u_k = i, j, k, components of velocity fluctuation
u_o = root mean square of velocity fluctuation Equation (1)
V_{avg} = time average mean voltage signal
ΔV = root mean square voltage fluctuation
ΔV_f = fraction of total root mean square voltage fluctuation per unit frequency step, that occurs at the chosen frequency n_f
v_i = volume of tap water fed into vessel per unit time
v_r = volume of fluid recirculated by impeller per unit time
v_t = volume of tracer fed into vessel per unit time
λ_c = Eulerian micro time scale for concentration fluctuations
λ_T = Eulerian micro time scale for velocity fluctuations
Φ = concentration fluctuation energy spectral distribution function based on frequency, Equation (6)

LITERATURE CITED

1. Batchelor, G. K., *J. Fluid Mech.*, **5**, 113 (1959).
2. ———, I. D. Howells, and A. A.. Townsend, *ibid.*, p. 134.
3. Beek, John, Jr., and R. S. Miller, *Chem. Eng. Progr., Symposium Ser. No. 25*, **55** (1959).
4. Brothman, A., *Chem. Met. Eng.*, **46**, 263 (1939).
5. Corrsin, Stanley, *A.I.Ch.E. Journal*, **3**, 329 (1957).
6. Foust, H. C., D. E. Mack, and J. H. Rushton, *Ind. Eng. Chem.*, **36**, 517 (1944).
7. Gutoff, E. B., *ibid.*, **48**, 1817 (1956).
8. Hill, J. B., *Chem & Met. Eng.*, **28**, 1077 (1923).
9. Hixson, A. W., *Ind. Eng. Chem.*, **36**, 488 (1944).
10. ———, A. H. Tenney, *Trans. Am. Inst. Chem. Engrs.*, **31**, 113 (1935).
11. Johnson, A. I., and C. J. Huang, *A.I.Ch.E. Journal*, **2**, 412 (1956).
12. Kramers, H., G. M. Baars, and W. H. Knoll, *Chem. Eng. Sci.*, **2**, 35 (1953).
13. Lamb, D. E., F. S. Manning, and R. H. Wilhelm, *A.I.Ch.E. Journal*, **6**, 682 (1960).
14. Liepmann, H. W., and M. S. Robinson, *Nat. Advisory Comm. Aeronaut. Tech. Note 3037* (1953).
15. MacDonald, R. W., and E. L. Piret, *Chem. Eng. Progr.*, **47**, 363 (1951).
16. Manning, F. S., Ph.D. dissertation, Princeton Univ., Princeton, New Jersey (1959).
17. Murphree, E. V., *Ind. Eng. Chem.*, **15**, 148 (1923).
18. Rodger, W. A., V. G. Trice, Jr., and J. H. Rushton, *Chem. Eng. Progr.*, **52**, 514 (1956).
19. Rushton, J. H., E. W. Costich, and H. J. Everett, *ibid.*, **46**, 395, 467 (1950).
20. van de Vusse, J. G., *Chem. Eng. Sci.*, **4**, 178 (1955).
21. White, A. M., S. D. Summerford, E. O. Bryant, and B. E. Lukens, *Ind. Eng. Chem.*, **24**, 1160 (1932).
22. Wood, J. C., E. R. Whittemore, and W. L. Badger, *Chem. & Met. Eng.*, **14**, 435 (1922).

Manuscript received June 16, 1960, revision received April 3, 1962; paper accepted April 9, 1962. Paper presented at A.I.Ch.E. San Francisco meeting.

Gaseous Counterdiffusion in Catalyst Pellets

LEONARD B. ROTHFELD

University of Wisconsin, Madison, Wisconsin

To assist in evaluating the role of internal pore diffusion in limiting the overall reaction rate in heterogeneous catalysis the rate of diffusion without reaction may be measured on the catalyst particle of interest, and an effective diffusion coefficient may be calculated. The convenient assumption is that the same effective diffusion coefficient applies to the differential equations for diffusion with chemical reaction under the same conditions of temperature, pressure, and chemical species. This approach was suggested by Damköhler (5) and expanded by Wheeler (27) and Wagner (25). An alternate approach of Thiele (23) has been less frequently used in recent research.

The effective diffusion coefficient depends on the properties of the gases, on the temperature and pressure, and on the pore structure of the catalyst. Since the measurements are made without chemical reaction, the measurement conditions must differ from the reaction conditions. The effective diffusion coefficient must be extrapolated over wide ranges of temperature and pressure and to different chemical species. To this end one often employs a tortuosity factor, which is the reciprocal of the ratio of the measured effective diffusion coefficient to the diffusion coefficient which applies to the fluid within the pores at the same conditions. It is then assumed that the tortuosity factor depends only on the catalyst pore structure.

Whether or not the tortuosity approximation is used, it cannot be disputed that an understanding of the diffusion mechanism within the pores is essential to the proper interpretation of diffusion data. This paper is intended to clarify that mechanism for the important case of binary gaseous diffusion.

L. B. Rothfeld is presently with the Shell Oil Company, Houston Research Laboratory, Deer Park, Texas.